A Unique and Simple Approach to Improve Sensitivity in ^{15}N-NMR Relaxation Measurements for NH$_3$$^+$ Groups: Application to a Protein-DNA Complex

Dan Nguyen[1], **Ganesh L.R. Lokesh**[2], **David E. Volk**[2], and **Junji Iwahara**[1,*]

[1]Department of Biochemistry and Molecular Biology, Sealy Center for Structural Biology and Molecular Biophysics, University of Texas Medical Branch, Galveston, TX 77555, USA

[2]McGovern Medical School, Brown Foundation Institute of Molecular Medicine for the Prevention of Human Diseases, University of Texas Health Science Center, Houston, TX 77030, USA

Abstract

NMR spectroscopy is a powerful tool for research on protein dynamics. In the past decade, there has been significant progress in the development of NMR methods for studying charged side chains. In particular, NMR methods for lysine side-chain NH$_3$$^+$ groups have been proven to be powerful for investigating the dynamics of hydrogen bonds or ion pairs that play important roles in biological processes. However, relatively low sensitivity has been a major practical issue in NMR experiments on NH$_3$$^+$ groups. In this paper, we present a unique and simple approach to improve sensitivity in ^{15}N relaxation measurements for NH$_3$$^+$ groups. In this approach, the efficiency of coherence transfers for the desired components are maximized, whereas undesired anti-phase or multi-spin order components are purged through pulse schemes and rapid relaxation. For lysine side-chain NH$_3$$^+$ groups of a protein-DNA complex, we compared the data obtained with the previous and new pulse sequences under the same conditions and confirmed that the ^{15}N relaxation parameters were consistent for these datasets. While retaining accuracy in measuring ^{15}N relaxation, our new pulse sequences for NH$_3$$^+$ groups allowed an 82% increase in detection sensitivity of ^{15}N longitudinal and transverse relaxation measurements.

Keywords

dynamics; ion pairs; NH$_3$$^+$ groups; NMR relaxation; protein side chains

---

*Correspondence: j.iwahara@utmb.edu; Tel.: +1-409-747-1403.

1. Introduction

NMR spectroscopy is one of the most powerful techniques for studying protein dynamics. NMR studies have revealed the functional importance of structural dynamics in many biological molecular processes of proteins (e.g., reviewed in Refs [1–8]). While the vast majority of NMR investigations of protein dynamics have probed motions of either backbone NH or side-chain CH_3 groups, NMR investigations on polar or charged side chains remain rare. Recently, there has been significant progress in NMR methods for investigating the dynamics of charged side chains of proteins [9–17]. In particular, NMR methods for Lys side-chain NH_3^+ groups have proven to be extremely useful for investigating the dynamics of hydrogen bonding and/or ion pairing [14–25].

Lys side-chain NH_3^+ groups of proteins undergo rapid hydrogen exchange with water [26–28]. As a result of this rapid hydrogen exchange, signals from NH_3^+ groups in ^1H-^{15}N heteronuclear single-quantum coherence (HSQC) and heteronuclear multiple-quantum coherence (HMQC) spectra are severely broadened [26]. Importantly, this broadening occurs not only in the ^1H dimension but also in the ^{15}N dimension, because rapid hydrogen exchange greatly enhances scalar relaxation of ^{15}N transverse coherence anti-phase with respect to ^1H (e.g., $2N_xH_z$, $4N_yH_zH_z$, and $8N_xH_zH_zH_z$).

To avoid this problem, Iwahara et al. developed NH_3^+-selective heteronuclear in-phase single-quantum coherence (HISQC) and its derivatives [26]. In the HISQC experiment, the in-phase single quantum term N_x or N_y is created at the beginning of the ^{15}N evolution period, and in-phase single-quantum coherence N_+ ($= N_x + iN_y$) is maintained via the ^1H WALTZ decoupling scheme throughout the evolution period. Evolutions to the anti-phase terms such as $2N_+H_z$, $4N_+H_zH_z$, and $8N_+H_zH_zH_z$ are suppressed to remove the impact of scalar relaxation on line shape of ^{15}N resonances. Scalar relaxation arises from auto-relaxation of the coupled ^1H nuclei [29,30], and substantially increases the relaxation rates of the $2N_+H_z$, $4N_+H_zH_z$, and $8N_+H_zH_zH_z$ terms, compared to the relaxation rates of N_+. The scalar relaxation rate R_{sc} for each ^1H nucleus is given by [26]:

$$R_{sc} = \rho_{HH} + k_{ex}^{water} \qquad (1)$$

where ρ_{HH} is the rate for dipole-dipole relaxation with external ^1H nuclei and k_{ex}^{water} is the rate for hydrogen exchange with water. Scalar relaxation rates for the N_+, $2N_+H_z$, $4N_+H_zH_z$, and $8N_+H_zH_zH_z$ terms are 0, R_{sc}, $2R_{sc}$, and $3R_{sc}$, respectively [31]. Typically, hydrogen exchange is much faster than ρ_{HH} rates and intrinsic ^{15}N relaxation rates for NH_3^+ groups [14–16,26]. Therefore, rapid hydrogen exchange governs relaxation of the anti-phase terms through the scalar relaxation mechanism and severely broadens ^{15}N line shapes of NH_3^+ signals in typical 2D ^1H-^{15}N correlation spectra. By maintaining in-phase single-quantum terms N_x and N_y, and thereby removing the scalar relaxation from the t_1 time domain for the ^{15}N dimension, the HISQC experiment drastically improved observation of ^1H-^{15}N cross peaks from NH_3^+ groups in sensitivity and resolution [26]. Since then, many NMR pulse sequences for NH_3^+ groups have implemented the principle of HISQC, and minimized the

adverse impacts of scalar relaxation of anti-phase terms with respect to ^{1}H nuclei [14–17,26,32].

Nevertheless, relatively low sensitivity due to rapid hydrogen exchange has been a major practical problem in NMR experiments for Lys side-chain NH_3^+ groups of proteins. While some side-chain NH_3^+ groups exhibit relatively slow hydrogen-exchange rates due to hydrogen bonds or ion pairs [26,33], many other NH_3^+ groups exhibit very rapid hydrogen-exchange rates that severely broaden ^{1}H resonances. Due to this problem, NMR experiments on protein side-chain NH_3^+ groups are often conducted at relatively low pH (typically pH 4.5–6.0) and low temperature (typically, 2–25 °C) to observe a larger number of signals with stronger intensity [32,34]. In these NMR experiments, co-axial NMR tubes that separate lock solvent (usually, D_2O) from a sample solution are typically used to avoid isotopically different species (i.e., NDH_2^+, and ND_2H^+, and ND_3^+) of NH_3^+ groups. The use of co-axial tubes further decreases sensitivity due to a smaller sample volume and multilayer glass walls. Thus, sensitivity improvement would be desirable for NMR experiments on NH_3^+ groups, especially for quantitative experiments such as ^{15}N relaxation measurements.

To address these practical needs, we present a unique and simple approach to improve sensitivity in ^{15}N relaxation measurements on protein side-chain NH_3^+ groups. Our approach involves only minor modifications of the existing pulse sequences. Nevertheless, the pulse sequences implementing this approach significantly improve the detection sensitivity, while maintaining the accuracy in the ^{15}N relaxation measurements on NH_3^+ groups.

2. Results

Figure 1 shows the optimized NMR pulse sequences for measuring [15]N R_1 and R_2 relaxation and heteronuclear NOE of NH_3^+ groups. In the description below, using the product operator formalism [35] for AX_3 spin systems, we first explain the previous approach that resolves problems arising from undesired anti-phase or multi-spin-order components of ^{15}N magnetizations of NH_3^+ groups in ^{15}N relaxation measurements. Then, we describe our new approach to improving sensitivity and eliminating undesired components in ^{15}N relaxation measurements, showing data that demonstrate the effectiveness of this approach.

2.1. Previous and Current Approaches to Eliminating the Adverse Effects of Multi-Spin Order Terms

The first step for measuring ^{15}N longitudinal (R_1) and transverse (R_2) relaxation rates is to create the ^{15}N in-phase single-quantum term via coherence transfer from ^{1}H to ^{15}N nuclei through a refocused INEPT scheme [39]. With regard to NH_3^+ groups, the product operator terms N_x, $2N_yH_z$, $4N_xH_zH_z$, and $8N_yH_zH_zH_z$ are generated in the period of $2\tau_b$ in the first refocused INEPT scheme of our pulse sequence for [15]N R_1 and R_2 measurements (Figure 1a,b). Because the only term of interest among them is N_x, any effects of the other three terms should be eliminated in these relaxation measurements. The $2N_yH_z$ and $8N_yH_zH_zH_z$ terms are eliminated by the pulsed field gradient (PFG) g_4 after the [1]H 90°(−x) and [15]N 90° (y) pulses at the end of the refocused INEPT scheme. These 90° pulses convert the N_x and $4N_xH_zH_z$ terms into N_z and $4N_zH_yH_y$, both of which survive the PFG g_4. The $4N_zH_yH_y$

term survives because a PFG alone cannot destroy homonuclear zero-quantum coherence [40]. To avoid any adverse impact of the $4N_xH_zH_z$ term generated in the refocused INEPT scheme, the previous pulse sequences used a value of the time τ_b that erases the $4N_xH_zH_z$ term, but retains the N_x term. This is possible because coherence transfer to these terms depends differently on the time τ_b. The coefficients of these transfers are given by [39]:

$$f_{CT}(2N_yH_z \rightarrow N_x) = \cos^2\theta\sin\theta \quad (2)$$

$$f_{CT}(2N_yH_z \rightarrow 4N_xH_zH_z) = (3\cos^2\theta - 1)\sin\theta \quad (3)$$

where $\theta = 2\pi J_{NH}\tau_b$ and $^1J_{NH}$ represents the one-bond ^{1}H-^{15}N scalar coupling constant. The use of the time τ_b satisfying $3\cos^2\theta - 1 = 0$ thus eliminates the $4N_xH_zH_z$ term, but retains the N_x term [15]. This approach was used for ^{13}C R_1 and R_2 relaxation measurements for protein CH_3 groups as well [41,42]. Because $^1J_{NH}$ is typically ~74 Hz for lysine side-chain NH_3^+ groups [26], the condition to suppress the $4N_xH_zH_z$ term was achieved using $\tau_b = 2.1$ ms in the original pulse sequences [15]. This condition was also used in the second refocused INEPT scheme for backward coherence transfer, so that any coherence transfer from $4N_xH_zH_z$ to $2N_yH_z$ does not contribute to the observed signals. A practical problem in using the condition of $f_{CT}(2N_yH_z \rightarrow 4N_xH_zH_z) = 0$ is that it also reduces $f_{CT}(2N_yH_z \rightarrow N_x)$ from its maximum level, and thereby weakens signals in the ^{15}N relaxation measurements for NH_3^+ groups (Figure 1d).

In the current work, we eliminate the adverse effects of the $4N_xH_zH_z$ term in a different manner, and maximize $f_{CT}(2N_yH_z \rightarrow N_x)$ to increase sensitivity in ^{15}N relaxation measurements for NH_3^+ groups. As shown in Figure 1d, the signal arising from the N_x term should be strongest when $\tau_b = 1.3$ ms. Although this condition increases the $4N_xH_zH_z$ term generated through the refocused INEPT scheme, our pulse sequences shown in Figure 1 prevent the undesired $4N_xH_zH_z$ term from becoming observable in the ^{1}H detection period t_1. This allows us to use $\tau_b = 1.3$ ms and improve sensitivity without compromising accuracy in ^{15}N relaxation measurements.

2.2. Assessment of the Sensitivity-Improved ^{15}N R_1 Experiment for NH_3^+ Groups

Our pulse sequence for the ^{15}N R_1 relaxation measurements on NH_3^+ groups is shown in Figure 1a. This pulse sequence is the same as that in Esadze et al. [15], except that the time τ_b is set to 1.3 ms instead of 2.1 ms. The ^{1}H 90°$(-x)$ and ^{15}N 90°(y) at the end of the first refocused INEPT convert the N_x and $4N_xH_zH_z$ terms into the N_z and $4N_zH_yH_y$ terms. As mentioned above, both of these terms survive the PFG g_4, and are subjected to the period T_r for relaxation measurement. For measuring ^{15}N R_1 relaxation rates, however, only the N_z term should be retained, and any contribution of the $4N_zH_yH_y$ term should be removed. During the period T_r, not only longitudinal relaxation, but also cross-correlation of three ^{1}H-^{15}N dipole-dipole (DD) relaxation mechanisms occur for the N_z term. The DD-DD cross-correlation causes partial transitions from N_z to $4N_zH_zH_z$ [43]. The composite of

water-selective [1]H 90°(−*x*) and hard [1]H 90°(*x*) pulses was originally introduced to prevent this term from becoming detectable while maintaining water ^{1}H magnetization along +*z* [15]. However, if a considerable amount of the $4N_zH_yH_y$ term is present at the beginning of the period T_r, the composite pulses at the end can partially convert this term into $4N_zH_zH_z$, which can survive the rest of the pulse sequence and become observable through the second refocused INEPT with $\tau_b = 1.3$ ms. This problem in the [15]N R_1 measurement can readily be resolved by taking advantage of rapid relaxation of the $4N_zH_yH_y$ term. Due to rapid hydrogen exchange with water, scalar relaxation of anti-phase and multi-spin order terms of [15]NH_3^+ are far faster than the intrinsic [15]N R_1 and R_2 relaxation of NH_3^+ groups [15,26]. Even under the conditions of pH 5.0 and 2 °C, where hydrogen exchange is relatively slow, the relaxation rates of the $4N_zH_zH_z$ term were ~20–100-fold faster than the relaxation rates of the N_z term for the Lys side-chain NH_3^+ groups of ubiquitin [15]. The relaxation of the $4N_zH_yH_y$ term should be even faster because of its transverse nature. Therefore, if the minimum duration of period T_r in the [15]N R_1 relaxation experiment is sufficiently long to let the $4N_zH_yH_y$ term completely decay, the relaxation rates of the N_z term (i.e., [15]N R_1) can be measured without any adverse contribution from the $4N_zH_yH_y$ term.

We applied this approach to the Lys side-chain NH_3^+ groups of the Antp homeodomain-DNA complex at pH 5.8 and 15 °C. The interfacial Lys side chains K46, K55, K57, and K58 of this protein-DNA complex exhibit well-resolved [1]H-^{15}N cross peaks in the NH_3^+-selective [1]H-^{15}N HISQC spectra (Figure 2). For these NH_3^+ groups, we measured [15]N R_1 relaxation rates with the previous and current pulse sequences using the same number of scans and data points. In these [15]N R_1 measurements, we recorded 2D [1]H-^{15}N spectra using $T_r = 100, 200, 400, 600, 900, 1200, 1600,$ and 2100 ms in an interleaved manner. The minimum duration, $T_r = 100$ ms, is expected to be long enough to let the $4N_zH_yH_y$ term completely decay through its rapid relaxation. As predicted in Figure 1d, the signals from NH_3^+ groups in the spectra recorded with $\tau_b = 1.3$ ms showed significantly stronger intensities than in those recorded with $\tau_b = 2.1$ ms. Figure 3a shows the signal intensity of the K46 NH_3^+ group as a function of T_r. The sensitivity was found to improve by a factor of 1.82 on average, which was consistent with the ratio of $|f_{CT}(2N_yH_z \rightarrow N_x)|^2$ at $\tau_b = 1.3$ ms and 2.1 ms. The ^{15}N relaxation rates R_1 were determined through nonlinear least-squares fitting with a single exponential function. Table 1 shows the [15]N R_1 relaxation rates measured with the previous and current pulse sequences for the Lys NH_3^+ groups in the Antp homeodomain-DNA complex. The [15]N R_1 rates from the two experiments were virtually the same, within experimental uncertainties. Not surprisingly, improvement in sensitivity led to higher precision in measured [15]N R_1 relaxation rates.

2.3. Assessment of the Sensitivity-Improved [15]N R_2 Experiment for NH_3^+ Groups

Our new pulse sequence for [15]N R_2 measurements is shown in Figure 1b. This pulse sequence differs from our previous one in two ways. First, $\tau_b = 1.3$ ms is used instead of $\tau_b = 2.1$ ms. Second, a composite of water-selective [1]H 90°(−*x*) and hard [1]H 90°(*x*) pulses is implemented before the PFG g_5. This additional component is important for canceling the effects of the $4N_yH_zH_z$ term generated through the refocused INEPT scheme. The pulse sequence uses the CW-CPMG scheme together with H_2O alignment pulse trains [37]. During the ^{15}N CPMG spin-echo periods for ^{15}N transverse relaxation measurements, a [1]H

continuous wave (CW) is applied at the ^{1}H resonances of NH_3^+ groups to maintain the in-phase single-quantum term N_x and prevent the anti-phase terms from being produced. Through the ^{1}H pulse scheme developed by Hansen et al. [37], water ^{1}H magnetization is aligned to the axis of ^{1}H CW in the rotating frame to avoid saturation through ^{1}H RF inhomogeneity and then is brought back to $+z$. Because this scheme does not align the $4N_zH_yH_y$ term, the terms arising from it are largely purged due to the RF inhomogeneity of the ^{1}H CW. However, their component parallel to the CW axis can remain and become the $4N_zH_zH_z$ term through the back-alignment scheme after the period T_r. Unlike the period T_r in the ^{15}N R_1 relaxation measurement, the period T_r in the ^{15}N R_2 relaxation measurement should be relatively brief, because only a limited number of hard ^{15}N 180° pulses can practically be used during the ^{15}N CPMG scheme. Therefore, this remaining undesired term cannot be purged completely through relaxation. However, the composite of the water-selective ^{1}H 90°$(-x)$ and hard ^{1}H 90°(x) pulses purges this $4N_zH_zH_z$ in the same manner as the $4N_zH_zH_z$ term arising from DD-DD cross-correlation during the period T_r is canceled in the ^{15}N R_1 measurement.

For the Lys side-chain NH_3^+ groups of the Antp homeodomain in complex with 15-bp DNA, we compared the ^{15}N R_2 relaxation data obtained with the old and new pulse sequences under the same conditions. We recorded nine ^{1}H-^{15}N spectra in an interleaved manner using T_r = 4.8, 14.4, 33.6, 48.0, 76.8, 91.2, and 105.6 ms. Strictly speaking, ^{15}N transverse relaxation of NH_3^+ groups should occur bi-exponentially due to DD-DD cross-correlation [15,41], but the first 30% decay from the maximum can be treated as a mono-exponential decay, as demonstrated by Esadze et al. [15]. Using mono-exponential fitting, the initial rate constants ($R_{2,ini}$) for this ^{15}N transverse relaxation were determined from the signal intensity as a function of T_r. The results from the data obtained with the previous and current pulse sequences are shown in Figure 3b and Table 1. The $R_{2,ini}$ rates from these two datasets are in good agreement. Due to the use of τ_b = 1.3 ms, the signal intensities in the spectra recorded with the current pulse sequence were significantly higher than those in the spectra recorded with the previous pulse sequence. As expected, the gain in intensity in the ^{15}N R_2 experiment was the same as that in the ^{15}N R_1 experiment (i.e., 82% increase on average). This improvement in sensitivity led to significantly higher precision in measured ^{15}N $R_{2,ini}$ rates.

2.4. Assessment of the Sensitivity-Improved Heteronuclear NOE Experiment for NH_3^+ Groups

Figure 1c shows the pulse sequence for heteronuclear NOE measurements for NH_3^+ groups that implements the abovementioned approach. As described by Esadze et al. [15], steady states of the N_z and $4N_zH_zH_z$ terms are created through saturation of ^{1}H nuclear magnetization via a train of 180° pulses for heteronuclear NOE measurements on NH_3^+ groups. The $4N_zH_zH_z$ steady state occurs due to DD-DD cross-correlation that drives transitions between the N_z and $4N_zH_zH_z$ terms [15]. In the original pulse sequence, τ_b = 2.1 ms was used to avoid any contribution of the $4N_zH_zH_z$ term to the observed signals. However, in the current pulse sequence (Figure 3c), the composite of the water-selective ^{1}H 90°$(-x)$ and hard ^{1}H 90°(x) pulses convert the $4N_zH_zH_z$ term into $4N_zH_yH_y$ immediately before the ^{15}N 90° pulse leading to the evolution period t_1. As described for the ^{15}N R_1 and

R_2 experiment, the rest of the pulse sequence does not allow the $4N_zH_yH_y$ term to become observable in the ^{1}H detection period t_2. Therefore, the use of $\tau_b = 1.3$ ms improves sensitivity without compromising the quality of heteronuclear NOE data, though the gain in sensitivity is relatively small because there is only a single refocused INEPT scheme in this pulse sequence.

We compared the heteronuclear NOE data obtained with the previous and current pulse sequences for the Lys NH_3^+ groups of the Antp homeodomain-DNA complex. Figure 3c shows ^{1}H slices of the 2D ^{1}H-^{15}N spectra recorded with and without ^{1}H saturation in the heteronuclear NOE experiments. The heteronuclear NOE values from the datasets obtained with the previous and current pulse sequences agreed well, as shown in Table 1. As expected, the spectra recorded with the new pulse sequence exhibited an increase in the intensity of each signal compared with those recorded with the previous pulse sequence under the same conditions. The improvement in the sensitivity was by a factor of 1.35 on average for the heteronuclear NOE measurements.

3. Discussion

As demonstrated above, our new pulse sequences improve sensitivity in ^{15}N relaxation measurements on protein side-chain NH_3^+ groups without compromising accuracy in measuring intrinsic ^{15}N relaxation parameters. By eliminating contributions from the undesired terms and maintaining the maximum level of coherence transfers of the desired terms, this method increased sensitivity by a factor of 1.82 for the R_1 and R_2 experiments and by a factor of 1.35 for the heteronuclear NOE experiment. Although our current paper shows data for a protein-DNA complex only, a similar degree of improvement is expected for other systems of different sizes because Equations (2) and (3) are independent of the molecular rotational correlation time. The sensitivity gains for the ^{15}N R_1 and R_2 experiments are larger because these experiments include two refocused INEPT schemes, whereas the heteronuclear NOE experiment has one. In fact, the relative magnitudes of the sensitivity gains (i.e., $1.82 \approx 1.35^2$) support this explanation. With the current approach, the time for recording the same quality of data can be significantly reduced compared with the previous ^{15}N relaxation experiments for NH_3^+ groups. The total measurement times for ^{15}N R_1 relaxation, R_2 relaxation, and heteronuclear NOE experiments on a 0.8 mM protein-DNA complex (17 kDa) were 18, 20, and 26 h, respectively. Note that signal to noise ratios are proportional to $\sqrt{N_s}$, where N_s is the number of accumulated scans per free induction decay (FID). To get the same data quality using the previous pulse sequences by increasing the number of scans, the total measurement times would approximately be tripled for ^{15}N R_1 and R_2 measurements and doubled for the heteronuclear NOE measurement. Because rapid hydrogen exchange of NH_3^+ groups weakens their ^{1}H signals, the improvement in sensitivity in these relaxation experiments is practically helpful. We hope that this approach will facilitate NMR studies of dynamic processes involving hydrogen bonds and ion pairs and help advance our understanding of protein dynamics and its functional roles.

4. Materials and Methods

The complex of the ^{15}N-labeled Antp homeodomain and unlabeled 15-bp DNA was prepared as described in our previous papers [21,25,44]. The DNA phosphate group at the K46 interaction site was dithioated in the chemical synthesis, as previously described [14,25]. A 370-μL solution of 0.8 mM complex in a buffer of 20 mM sodium phosphate (pH 5.8) and 20 mM NaCl was sealed in a 5-mm outer tube of a co-axial NMR tube system. To avoid the deuterated species of NH_3^+ groups (i.e., NDH_2^+, ND_2H^+, and ND_3^+), D_2O for the NMR lock signal was sealed separately in an inter insert of the co-axial tube. The NMR experiments were performed at 15 °C with a Bruker Avance III spectrometer operated at the ^{1}H frequency of 750 MHz. A TCI cryogenic probe was used for NMR detection. The ^{1}H and ^{15}N acquisition times were 54 ms and 222 ms, respectively. In each experiment, 16 scans were accumulated per FID, and sub-spectra were recorded in an interleaved manner. The NMR data were processed and analyzed using the NMR-Pipe [45] and NMR-View [46] programs. Other experimental details are given in figure captions.

Acknowledgments

References

1. Boehr DD, Dyson HJ, Wright PE. An NMR perspective on enzyme dynamics. Chem Rev. 2006; 106:3055–3079. [PubMed: 16895318]

2. Clore GM, Iwahara J. Theory, practice, and applications of paramagnetic relaxation enhancement for the characterization of transient low-population states of biological macromolecules and their complexes. Chem Rev. 2009; 109:4108–4139. [PubMed: 19522502]

3. Kalodimos CG. NMR reveals novel mechanisms of protein activity regulation. Protein Sci. 2011; 20:773–782. [PubMed: 21404360]

4. Kay LE. New views of functionally dynamic proteins by solution NMR spectroscopy. J Mol Biol. 2016; 428:323–331. [PubMed: 26707200]

5. Loria JP, Berlow RB, Watt ED. Characterization of enzyme motions by solution NMR relaxation dispersion. Acc Chem Res. 2008; 41:214–221. [PubMed: 18281945]

6. Palmer AG III. NMR probes of molecular dynamics: Overview and comparison with other techniques. Annu Rev Biophys Biomol Struct. 2001; 30:129–155. [PubMed: 11340055]

7. Villali J, Kern D. Choreographing an enzyme's dance. Curr Opin Chem Biol. 2010; 14:636–643. [PubMed: 20822946]

8. Wand AJ. The dark energy of proteins comes to light: Conformational entropy and its role in protein function revealed by NMR relaxation. Curr Opin Struct Biol. 2013; 23:75–81. [PubMed: 23246280]

9. Stafford KA, Ferrage F, Cho JH, Palmer AG III. Side chain dynamics of carboxyl and carbonyl groups in the catalytic function of Escherichia coli ribonuclease H. J Am Chem Soc. 2013; 135:18024–18027. [PubMed: 24219366]

10. Paquin R, Ferrage F, Mulder FA, Akke M, Bodenhausen G. Multiple-Timescale dynamics of side-chain carboxyl and carbonyl groups in proteins by ^{13}C nuclear spin relaxation. J Am Chem Soc. 2008; 130:15805–15807. [PubMed: 18975903]

11. Hansen AL, Kay LE. Quantifying millisecond time-scale exchange in proteins by CPMG relaxation dispersion NMR spectroscopy of side-chain carbonyl groups. J Biomol NMR. 2011; 50:347–355. [PubMed: 21681650]

12. Werbeck ND, Kirkpatrick J, Hansen DF. Probing arginine side-chains and their dynamics with carbon-detected NMR spectroscopy: Application to the 42 kDa human histone deacetylase 8 at high pH. Angew Chem Int Ed Engl. 2013; 52:3145–3147. [PubMed: 23401322]

13. Trbovic N, Cho JH, Abel R, Friesner RA, Rance M, Palmer AG III. Protein side-chain dynamics and residual conformational entropy. J Am Chem Soc. 2009; 131:615–622. [PubMed: 19105660]

14. Anderson KM, Esadze A, Manoharan M, Brüschweiler R, Gorenstein DG, Iwahara J. Direct observation of the ion-pair dynamics at a protein-DNA interface by NMR spectroscopy. J Am Chem Soc. 2013; 135:3613–3619. [PubMed: 23406569]

15. Esadze A, Li DW, Wang T, Brüschweiler R, Iwahara J. Dynamics of lysine side-chain amino groups in a protein studied by heteronuclear ^{1}H-^{15}N NMR spectroscopy. J Am Chem Soc. 2011; 133:909–919. [PubMed: 21186799]

16. Zandarashvili L, Esadze A, Iwahara J. NMR studies on the dynamics of hydrogen bonds and ion pairs involving lysine side chains of proteins. Adv Protein Chem Struct Biol. 2013; 93:37–80. [PubMed: 24018322]

17. Zandarashvili L, Li DW, Wang T, Brüschweiler R, Iwahara J. Signature of mobile hydrogen bonding of lysine side chains from long-range ^{15}N-^{13}C scalar J-couplings and computation. J Am Chem Soc. 2011; 133:9192–9195. [PubMed: 21591797]

18. Chen CY, Esadze A, Zandarashvili L, Nguyen D, Pettitt BM, Iwahara J. Dynamic equilibria of short-range electrostatic interactions at molecular interfaces of protein-DNA complexes. J Phys Chem Lett. 2015; 6:2733–2737. [PubMed: 26207171]

19. Iwahara J, Esadze A, Zandarashvili L. Physicochemical properties of ion pairs of biological macromolecules. Biomolecules. 2015; 5:2435–2463. [PubMed: 26437440]

20. Esadze A, Chen C, Zandarashvili L, Roy S, Pettitt BM, Iwahara J. Changes in conformational dynamics of basic side chains upon protein-DNA association. Nucleic Acids Res. 2016; 44:6961–6970. [PubMed: 27288446]

21. Nguyen D, Zandarashvili L, White MA, Iwahara J. Stereospecific effects of oxygen-to-sulfur substitution in DNA phosphate on ion pair dynamics and protein-DNA affinity. Chembiochem. 2016; 17:1636–1642. [PubMed: 27271797]

22. Zandarashvili L, Esadze A, Kemme CA, Chattopadhyay A, Nguyen D, Iwahara J. Residence times of molecular complexes in solution from NMR data of intermolecular hydrogen-bond scalar coupling. J Phys Chem Lett. 2016; 7:820–824. [PubMed: 26881297]

23. Zandarashvili L, Esadze A, Vuzman D, Kemme CA, Levy Y, Iwahara J. Balancing between affinity and speed in target DNA search by zinc-finger proteins via modulation of dynamic conformational ensemble. Proc Natl Acad Sci USA. 2015; 112:E5142–E5149. [PubMed: 26324943]

24. Zandarashvili L, Iwahara J. Temperature dependence of internal motions of protein side-chain NH$_3$$^+$ groups: Insight into energy barriers for transient breakage of hydrogen bonds. Biochemistry. 2015; 54:538–545. [PubMed: 25489884]

25. Zandarashvili L, Nguyen D, Anderson KM, White MA, Gorenstein DG, Iwahara J. Entropic enhancement of protein-DNA affinity by oxygen-to-sulfur substitution in DNA phosphate. Biophys J. 2015; 109:1026–1037. [PubMed: 26331260]

26. Iwahara J, Jung YS, Clore GM. Heteronuclear NMR spectroscopy for lysine NH$_3$ groups in proteins: Unique effect of water exchange on ^{15}N transverse relaxation. J Am Chem Soc. 2007; 129:2971–2980. [PubMed: 17300195]

27. Liepinsh E, Otting G. Proton exchange rates from amino acid side chains—Implications for image contrast. Magn Reson Med. 1996; 35:30–42. [PubMed: 8771020]

28. Segawa T, Kateb F, Duma L, Bodenhausen G, Pelupessy P. Exchange rate constants of invisible protons in proteins determined by NMR spectroscopy. Chembiochem. 2008; 9:537–542. [PubMed: 18247446]

29. Abragam, A. The Principle of Nuclear Magnetism. Carendon Press; Oxford, UK: 1961. Thermal relaxation in liquids and gases; p. 264-353.

30. Bax A, Ikura M, Kay LE, Torchia DA, Tschudin R. Comparison of different modes of two-dimensional reverse-correlation NMR for the study of proteins. J Magn Reson. 1990; 86:304–318.

31. Ollerenshaw JE, Tugarinov V, Kay LE. Methyl TROSY: Explanation and experimental verification. Magn Reson Chem. 2003; 41:843–852.

32. Esadze A, Zandarashvili L, Iwahara J. Effective strategy to assign ^{1}H-^{15}N heteronuclear correlation NMR signals from lysine side-chain NH_3^+ groups of proteins at low temperature. J Biomol NMR. 2014; 60:23–27. [PubMed: 25129623]

33. Poon DK, Schubert M, Au J, Okon M, Withers SG, McIntosh LP. Unambiguous determination of the ionization state of a glycoside hydrolase active site lysine by ^{1}H-^{15}N heteronuclear correlation spectroscopy. J Am Chem Soc. 2006; 128:15388–15389. [PubMed: 17132001]

34. Wüthrich, K. NMR of Proteins and Nucleic Acids. Wiley-Interscience; New York, NY, USA: 1986. p. 23-25.

35. Sørensen OW, Eich GW, Levitt MH, Bodenhausen G, Ernst RR. Product operator-formalism for the description of NMR pulse experiments. Prog Nucl Magn Reson Spectrosc. 1983; 16:163–192.

36. Kup e E, Boyd J, Campbell ID. Short selective pulses for biochemical applications. J Magn Reson Ser B. 1995; 106:300–303. [PubMed: 7719630]

37. Hansen DF, Vallurupalli P, Kay LE. An improved ^{15}N relaxation dispersion experiment for the measurement of millisecond time-scale dynamics in proteins. J Phys Chem B. 2008; 112:5898–5904. [PubMed: 18001083]

38. Hansen DF, Kay LE. Improved magnetization alignment schemes for spin-lock relaxation experiments. J Biomol NMR. 2007; 37:245–255. [PubMed: 17310328]

39. Ernst, RR., Bodenhausen, G., Wokaun, A. Principles of Nuclear Magnetic Resonance in One and Two Dimensions. Oxford University Press; New York, NY, USA: 1987. Heteronuclear polarization transfer; p. 180-201.

40. Van de Ven, FJM. Multidimensional NMR in Liquids: Basic Principles and Experimental Methods. VCH Publishers; New York, NY, USA: 1995. Dephasing coherences; p. 211-224.

41. Kay LE, Bull TE, Nicholson LK, Griesinger C, Schwalbe H, Bax A, Torchia DA. The measurement of heteronuclear transverse relaxation-times in AX3 spin systems via polarization-transfer techniques. J Magn Reson. 1992; 100:538–558.

42. Palmer AG, Wright PE, Rance M. Measurement of relaxation-time constants for methyl-groups by proton-detected heteronuclear NMR spectroscopy. Chem Phys Lett. 1991; 185:41–46.

43. Kumar A, Grace RCR, Madhu PK. Cross-Correlations in NMR. Prog NMR Spect. 2000; 37:191–319.

44. Anderson KM, Nguyen D, Esadze A, Zandrashvili L, Gorenstein DG, Iwahara J. A chemical approach for site-specific identification of NMR signals from protein side-chain NH_3^+ groups forming intermolecular ion pairs in protein-nucleic acid complexes. J Biomol NMR. 2015; 62:1–5. [PubMed: 25690740]

45. Delaglio F, Grzesiek S, Vuister GW, Zhu G, Pfeifer J, Bax A. NMRPipe: A multidimensional spectral processing system based on UNIX pipes. J Biomol NMR. 1995; 6:277–293. [PubMed: 8520220]

46. Johnson BA, Blevins RA. NMR view: A computer-program for the visualization and analysis of NMR data. J Biomol NMR. 1994; 4:603–614. [PubMed: 22911360]
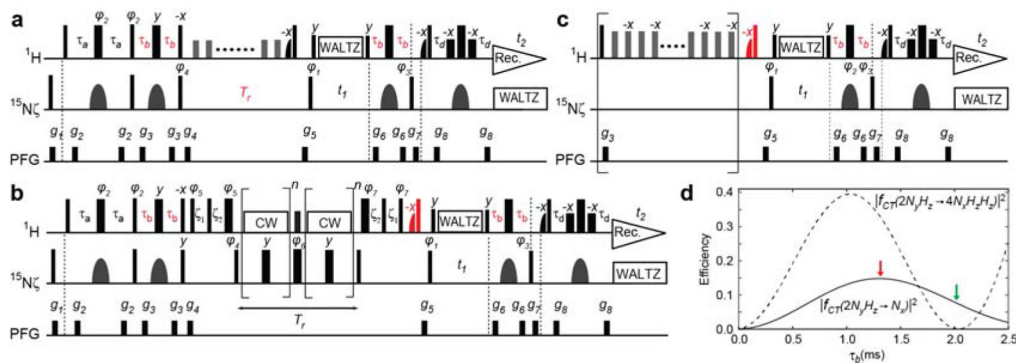
Figure 1.

Pulse sequences for the ^{15}N relaxation measurement on lysine side-chain NH_3^+ groups. The key elements in the current work are indicated in red. Thin and bold bars in black represent hard rectangular 90° and 180° pulses, respectively. Water-selective half-Gaussian (2.1 ms) and soft-rectangular (1.2 ms) 90° pulses are represented by half-bell and short-bold shapes, respectively. Unless indicated otherwise, pulse phases are along x, and the carrier position for ^1H was set to the position of the water resonance. The ^{15}N carrier position was set to 33.1 ppm. A gray bell-shape for ^{15}N represents an r-SNOB[36] 180° pulse (1.0 ms) selective to Lys side-chain $^{15}N_\zeta$ nuclei. The delays τ_a and τ_b were 2.7 ms and 1.3 ms, respectively. Quadrature detection in the t_1 domain was achieved using States-TPPI, incrementing the phase φ_1. Pulsed field gradients (PFGs) were optimized to minimize the water signal. (**a**) ^{15}N R_1 measurement. Although it is not essential owing to negligible CSA-DD cross correlation for NH_3^+, a ^1H 180° pulse, which does not affect H_2O resonance, was applied every 10 ms during the delay T_r for longitudinal relaxation. Phase cycles: $\varphi_1 = (2y, 2(-y))$, $\varphi_2 = (y, -y)$, $\varphi_3 = (4x, 4(-x))$, $\varphi_4 = (8y, 8(-y))$, and receiver $= (x, -x, -x, x, 2(-x, x, x, -x), x, -x, -x, x)$; (**b**) ^{15}N $R_{2,ini}$ measurement. The RF strength for ^{15}N pulses for the CPMG scheme was 5.4 kHz. The ^1H carrier position was shifted to 7.8 ppm right after the PFG g_4 and set back to the position of water resonance right after the PFG g_5. The RF strength $\omega_{CW}/2\pi$ of ^1H CW during the CPMG was set to 4.3 kHz, which was adjusted to satisfy $\omega_{CW}/2\pi = 2k\nu_{CPMG}$ (k, integer) [37]. The delays ξ_1 and ξ_2 are for alignment of ^1H magnetization and given by $\xi_1 = 1/\omega_{CW} - (4/\pi)\tau_{90H}$ and $\xi_2 = \tau_{90N} - (2/\pi)\tau_{90H}$ [37,38], in which τ_{90} represents a length of a relevant 90° pulse. Phase cycles: $\varphi_1 = (4y, 4(-y))$, $\varphi_2 = (8y, 8(-y))$, $\varphi_3 = x$, $\varphi_4 = (x, -x)$, $\varphi_5 = (2y, 2(-y))$, $\varphi_6 = (2x, 2(-x))$, $\varphi_7 = (2(-y), 2y)$, and receiver $= (x, -x, x, -x, 2(-x, x, -x, x), x, -x, x, -x)$; (**c**) Heteronuclear ^1H-^{15}N NOE measurement. Measurement with ^1H saturation (5 s) was performed with a train of $180°x$ and $180°(-x)$ pulses (RF strength, 11 kHz) at an interval of 10 ms. The ^1H carrier position was at 7.8 ppm during the ^1H saturation period. The reference spectrum was measured without the scheme in the bracket. The recycle delay (including the saturation period) was set to 18 s for a 750-MHz spectrometer. Phase cycles: $\varphi_1 = (y, -y)$, $\varphi_2 = (4x, 4y, 4(-x), 4(-y))$, $\varphi_3 = (2x, 2(-x))$, and receiver $= (x, -x, -x, x, -x, x, x, -x)$; (**d**) Efficiency in coherence transfers as a function of the delay τ_b calculated using Equations (2) and (3) with $|^1J_{NH}| = 74$ Hz and ^1H 180° pulse length of 20 μs. The results for the N_y and $4N_yH_zH_z$ terms are shown in solid and dotted lines, respectively. Red and green arrows indicate the values of the delay τ_b in the current and previous pulse sequences, respectively.
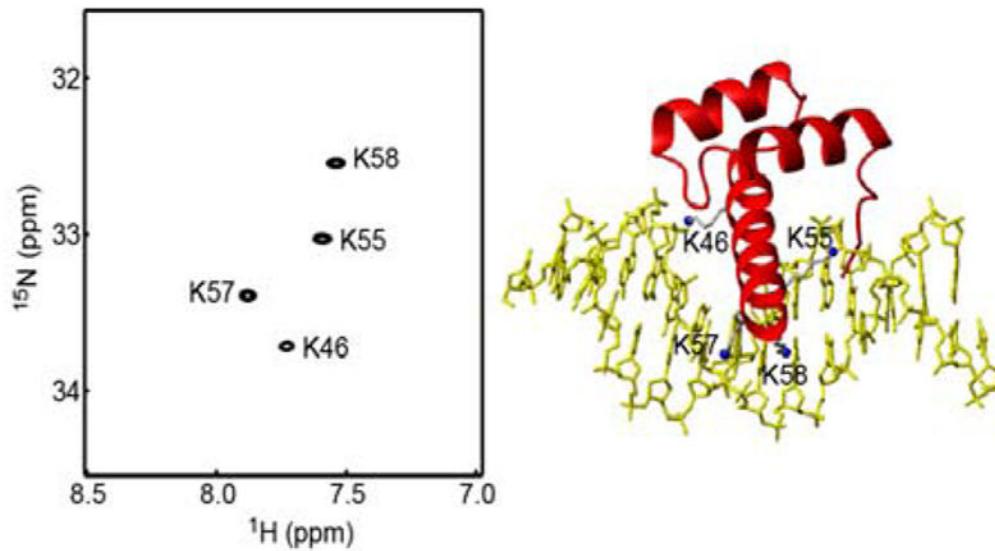
Figure 2.
The ^{1}H-^{15}N HISQC spectrum recorded at 15 °C for the NH_3^+ groups in the complex of ^{15}N-labeled Antp homeodomain and unlabeled 15-bp DNA containing a phosphorodithioate at the K46 interaction site. The resonance assignment is based on that for the unmodified DNA complex and unique chemical shift perturbation upon site-specific dithioation (i.e., sulfur substitutions of two non-bridging oxygen atoms) of the DNA phosphate at the K46 interaction site [44].
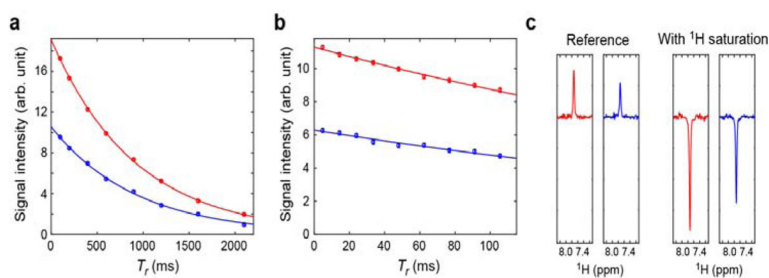
Figure 3.
Comparison of the previous [15] and current pulse sequences for measuring ^{15}N relaxation of NH_3^+ groups. (**a,b**) ^{15}N longitudinal (Panel **a**) and transverse (Panel **b**) relaxation of the K46 NH_3^+ group. The vertical axis represents the signal intensity in the two-dimensional spectra measured as a function of the relaxation period T_r. Solid lines represent the best-fit curves obtained through nonlinear least-squares fitting with a mono-exponential function; (**c**) Slices of the K46 NH_3^+ signals along the ^{1}H dimension from the two-dimensional spectra with and without ^{1}H saturation for the heteronuclear NOE measurements. In each panel, data obtained with the previous and current pulse sequences are shown in blue and red, respectively.

Table 1

Comparison of ^{15}N relaxation parameters measured with the previous and current pulse sequences [a]. Shown below are data for the Lys side-chain NH_3^+ groups in the complex of ^{15}N-labeled Antp homeodomain and unlabeled 15-bp DNA containing a phosphorodithioate at the K46 interaction site.

	K46	K55	K57	K58
^{15}N R_1 (s^{-1}) [b]	1.093 ± 0.013	0.637 ± 0.005	1.035 ± 0.004	0.363 ± 0.002
^{15}N R_1 (s^{-1}) [c]	1.081 ± 0.023	0.617 ± 0.008	1.037 ± 0.008	0.364 ± 0.003
^{15}N $R_{2,ini}$ (s^{-1}) [b]	2.55 ± 0.10	1.76 ± 0.07	2.95 ± 0.04	1.20 ± 0.03
^{15}N $R_{2,ini}$ (s^{-1}) [c]	2.74 ± 0.20	2.05 ± 0.12	2.76 ± 0.06	1.14 ± 0.06
Heteronuclear NOE [b]	−2.44 ± 0.12	−2.83 ± 0.10	−2.54 ± 0.05	−2.71 ± 0.05
Heteronuclear NOE [c]	−2.53 ± 0.18	−2.75 ± 0.13	−2.60 ± 0.08	−2.65 ± 0.07

[a] The experiments were conducted at 15 °C and the ^1H frequency of 750 MHz. Uncertainties were estimated using the Monte Carlo approach based on the noise standard deviation of the spectra.

[b] Measured with the current pulse sequences shown in Figure 1.

[c] Measured with the previous pulse sequences [15].